Proceedings of the ASME 2021
Internal Combustion Engine Division Fall Technical Conference
ICEF2021
October 13-15, 2021, Virtual, Online

ICEF2021-66745

BOOSTING THE CAPABILITIES OF GAS STAND DATA ACQUISITION AND CONTROL SYSTEMS BY USING A DIGITAL TWIN BASED ON A HOLISTIC TURBOCHARGER MODEL

José R. Serrano
CMT-Motores Térmicos
Universitat Politècnica de València
Valencia 46022, Spain
Email: jrserran@mot.upv.es

Luis Miguel García-Cuevas
CMT-Motores Térmicos
Universitat Politècnica de València
Valencia 46022, Spain
Email: luiga12@mot.upv.es

Vishnu Samala
CMT-Motores Térmicos
Universitat Politècnica de València
Valencia 46022, Spain
Email: vishnu.sunsea@gmail.com

Juan Antonio López-Carrillo
CMT-Motores Térmicos
Universitat Politècnica de València
Valencia 46022, Spain
Email: jualoca6@mot.upv.es

Holger Mai
Kratzer Automation AG
Eichendorffstrasse 20,
D-38440 Wolfsburg, Germany
Email: holger.mai@kratzer-automation.com

ABSTRACT

During the last decade, increasingly advanced turbocharger models have been developed for sizing, engine matching and one-dimensional modeling. This work goes further and, instead of using these models for turbocharged engines design or analysis, it implements them in the data acquisition and control system of a turbocharger gas stand. This way, interesting new capabilities arise. The paper shows that there are important synergies between advanced turbocharger gas stand data acquisition and control systems and the modern turbocharger holistic models that have not been deeply exploited until now. They can be summarized as: on-line heat fluxes analysis, in-situ outlier testing points detection, testing time saving and using digital-twin techniques to monitor turbocharger health during testing.

Keywords: Turbocharger testing, heat transfer, adiabatic maps, friction losses, data acquisition, data postprocessing and analysis.

NOMENCLATURE

c_p	Specific heat capacity [J kg^{-1} K^{-1}]
F	Force [N]
$\dot{m}$	Mass flow [kg s^{-1}]
N	Rotational speed [rpm]
$\dot{Q}$	Heat transfer [W]
T	Temperature [K]
$T\#1$	Turbocharger measured in hot conditions
$T\#2$	Turbocharger measured in cold conditions
$\dot{W}$	Power [W]

Superscript

ad	Adiabatic conditions
C	Compressor
exp	Experimental results
model	Model results
T	Turbine

Subscript

ad	Adiabatic conditions
C	Compressor
C/Air	Compressor to air side
corr	Corrected
ETE	Effective turbine efficiency
exp	Experimental results
hot	Hot conditions
Gas/T	Turbine to gas side
mech	Mechanical
ml	Friction losses

model	Model results
0	Static outlet conditions
0I	Oil inlet conditions
oil	Lube oil
red	Reduced
s	Isentropic conditions
T	Turbine
t/s	Total to static conditions
t/t	Total to total conditions
TI	Total inlet conditions
TO	Total outlet conditions
WI	Water inlet conditions

Greek letters

δ	Relative percentage error
η	Corresponding efficiency
μ	Dynamic viscosity
Π	Pressure ratio
σ	Blade-to-jet speed ratio

Abbreviations

BSR	Blade-to-jet speed ratio [-]
ETE	Effective turbine efficiency [-]
ICE	Internal Combustion Engine

1. INTRODUCTION

Several works have already pointed the importance of considering heat transfer aspects in the turbocharger [1]. Considering the turbocharger heat transfer phenomena in a whole one-dimensional engine simulation of transient cycles improve the turbocharger model prediction capabilities in terms of precision and robustness [2]. Particularly, to compute the turbine and compressor outlet temperatures and machine powers, as they depend on the turbine and compressor adiabatic efficiencies [3]. During the last decades, increasingly advanced turbocharger models have been developed for sizing, engine matching and one-dimensional modeling [4]. All the interesting phenomena are currently considered with high accuracy: adiabatic map extrapolation of both turbine [4] and compressor [5], friction losses [6] and heat transfer effects [7], can be computed hundreds of times per second with commodity hardware. All of these sub-models are based on zero- or one-dimensional approaches and are used in a whole engine model simulation to improve the predictions [8]. This work goes further and, instead of using these models for engine design or modeling for analysis purposes, it implements them in the data acquisition and control system of a turbocharger gas stand. This way, interesting new capabilities arise. On-line adiabatization of the turbocharger maps make them easy to use in standard one-dimensional engine simulation software packages, coupled with heat transfer sub models. Comparing the measured maps with extrapolated data can be used to decide when the data density and extension is enough to be used in one-dimensional engine modeling, optimizing the time needed for characterization. Possible outliers and sensor failures can be detected if there are important differences between the measured data points and the adiabatic, interpolated, and extrapolated output from the models. Hydrodynamic friction model results can be compared with measurement data to alert of direct metal-to-metal contact in the bearings. This happens due to, for example, very high axial loads, such as when using a pressurized compressor closed loop. Also, metal-to-metal contact can happen when oil has been deteriorated because of high temperature operation, such as when performing quasi-adiabatic tests [9]. These tests are needed because several reasons, for example, in these conditions mechanical losses power can be directly estimated from measured data by using Eqn. (1). Despite the already mentioned damage that oil could suffer, there are some advantages in testing turbochargers this way, such as the possibility of directly estimating the mechanical losses power from measured data and fluid properties using Eqn. (1).

$$\dot{W}_{\mathrm{ml,exp}} = \dot{m}_{\mathrm{oil}} \cdot c_p^{\mathrm{oil}} \cdot \Delta T_{\mathrm{oil}} \qquad (1)$$

Therefore, there are important synergies between advanced turbocharger gas stand data acquisition and control systems and the modern turbocharger holistic models that are explored in this work. Sections 2 and 3 include a description of the gas stand used for the tests and industry-standard compressor and turbine mapping procedures. Section 4 briefly describes the holistic turbocharger model coupled with the gas stand control software. Section 5 describes the results of adiabatizing two variable geometry turbine (VGT) turbochargers measured with two techniques, i.e., T#1 was measured using a standard hot test with high turbine inlet gas temperature and T#2 was measured at quasi-adiabatic conditions. Section 5 also analyses the heat fluxes, which can be an additional output of the gas stand and compares pure adiabatized maps (postprocessed results) with the two types of tests. Section 6 shows how can be used the adiabatized and extrapolated maps to save time (and money) by reducing the number of needed testing points when this type of maps must be generated at a gas-stand. Section 7 shows an example and the analysis of how the hydrodynamic friction model can be used as a digital-twin to alert of direct metal-to-metal contact in the bearings. Finally, Section 7 concludes about the paper findings.

2. TURBOCHARGER GAS STAND

The hot gas stand is designed for testing turbochargers. Compressor and turbine mapping are the most typical gas stand use cases that are normally performed in a compressor open-loop configuration using compressor back pressure valves (COLU) as shown in Fig 1. The gas stand and the measurement technology correspond to the current state of the art for evaluating the performance and efficiency of turbochargers. The core component of the gas stand is a high-temperature combustion chamber powered by natural gas, which can be used to generate

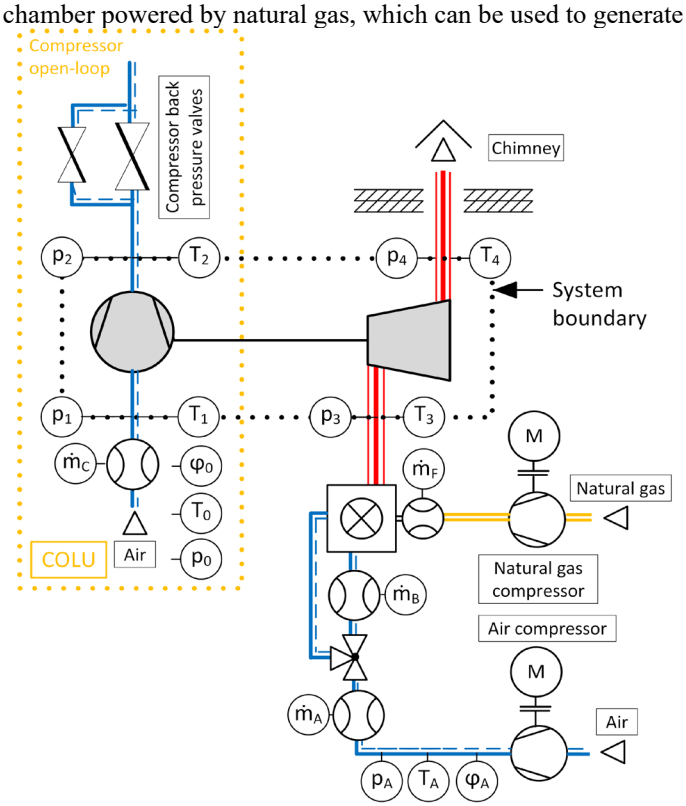

FIG 1: STANDARD GAS STAND APPLICATION FOR COMPRESSOR AND TURBINE MAPPING.

hot gas temperatures up to 1200°C. This enables turbocharger testing for maximum turbine inlet temperature of T_3=1050°C. The additional conditioning systems for oil supply and cooling water allow to test turbochargers under close to the engine conditions. As shown schematically in Fig 1, compressed air is applied to the turbine inlet of the turbocharger on the gas stand. The combustion chamber runs lambda-controlled. There are several control loops in the automation system for controlling the turbine inlet state of the turbocharger in semi-automatic and fully-automatic operation modes.

The control loops for controlling the gas temperature at the turbine inlet are the power control and the temperature control. The combustion chamber power can be varied by the natural gas supply. For the temperature control the mixed air valve is used to control the combustion chamber outlet or turbine inlet temperature very accurate with high dynamic response. The control loops for controlling the mass flow at turbine inlet allows to control the turbine mass flow directly or indirectly with the turbocharger speeds, such as the physical speed, the circumferential speed, or any corrected speed.

On the compressor side all control loops for controlling the compressor outlet state are using the compressor back pressure valves downstream of the compressor. The typical control loops are the mass flow control and the control of the compressor pressure ratio in order to be able to measure the stable operating range of the radial compressor from the surge to the choke limit.

The combustion chamber feeds the turbine with hot gas at a certain pressure and temperature level. The turbine is driven by the exhaust gas enthalpy. The turbine converts the gas energy into mechanical shaft power to drive the compressor. The compressor densifies the intake air from ambient conditions to a higher pressure and temperature level. As shown in Fig 1, the compressor back pressure valves are used to set the desired compressor operating point under steady-state conditions.

The system boundary of the turbocharger is represented by the pressure tapping points for measuring the static pressure and the position of the temperature sensors in the measurement sections upstream and downstream of the compressor and turbine, indicated by the positions 1, 2, 3 and 4.

3. COMPRESSOR AND TURBINE MAPPING

Basically, the compressor and turbine maps are indicating the possible operating range of the turbocharger for the internal combustion engine (ICE). The main purpose for turbocharger testing on a gas stand is to measure compressor and turbine maps in a wide range under specific boundary conditions for the thermodynamic evaluation. Compressor and turbine mapping are usually performed in automatic mapping sequences controlled and monitored by the gas stand automation system.

For the automatic mapping process, the turbocharger characteristics are calculated for the compressor and turbine with respect to pre-defined stability criteria on the gas stand to achieve steady-state conditions. The characterization of specific points is necessary to provide a starting point, and the limits of the characteristic maps for compressor and turbine (choke point, surge point and the point with maximum turbine power) for each speed line. The maps are measured at different constant speeds with usually 8 to 12 operating points per speed line. In each operating point, the turbocharger states are measured and the characteristics for compressor and turbine are calculated with respect to the stability criteria on the gas stand in order to achieve steady-state thermodynamic conditions and then store the current operating point.

During steady-state compressor and turbine mapping, heat fluxes occur and can have a significant impact on the compressor and turbine efficiencies which are usually not considered for assessing the turbocharger mapping quality. So-called standard mapping for evaluating a turbocharger on the gas stand is carried out in accordance with SAE guideline J1826 [10] which is intended to simulate engine operation in real vehicle application on the gas stand with simplifications. The standard mapping is performed with constant turbine inlet temperature of T_3=600°C and constant oil inlet temperature of T_{oil}=90°C. There is no insulation of the measurement sections. Despite, this methodology seems to be standard, there are some disadvantages for the compressor mapping as shown in Fig 2. The impact of heat fluxes is most relevant at low speeds and mass flows and can lead to heat up the process gas. For standard mapping, indicated as hot in Fig 2, at low speeds thermal power coming from the oil system is relatively large in relation to the effective compressor power and is added to the already heated process gas. This results in a further increase in the measured temperature at the compressor outlet at the system boundary, which is not caused by the actual compression process itself and lowers the compressor efficiency significantly. In comparison to the hot curves, the quasi-adiabatic curves in Fig 2 show the aerodynamic compressor efficiency which is not affected by heat fluxes. Only at higher speeds heat fluxes can be neglected.

From the customer's point of view, it is definitely relevant under which boundary conditions the maps are determined on the gas stand. Since the customer has high demands on the mapping quality, the results based on measurement methodology should be as close as possible to the aerodynamic efficiencies of the compressor and turbine for all speeds in fully automatic gas stand operation. However, the implementation of quasi-adiabatic mapping on the gas stand is very complex, requires more operating time and has so far been comparatively costly. This is still less economical compared to standard hot mapping according to SAE, which has so far represented the best compromise in terms of measurement quality and comparability with other gas stands. Therefore, further gas stand investigations should combine the qualitative advantages of the quasi-adiabatic mapping methodology with the economic advantages of the standard hot mapping methodology.

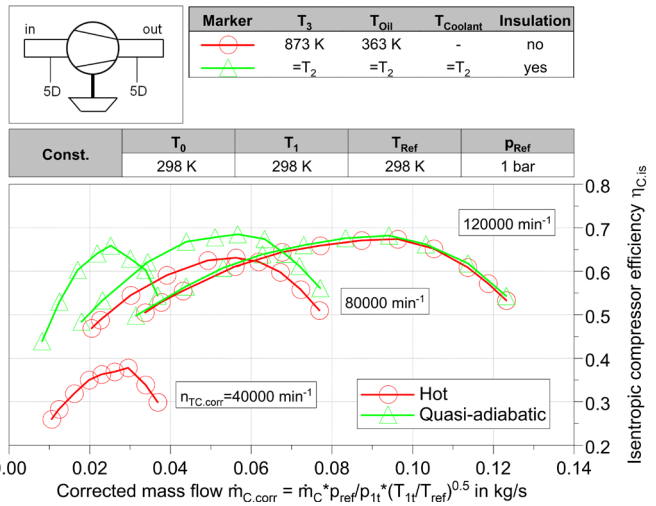

FIG 2: IMPACT OF MEASUREMENT METHODOLOGY ON COMPRESSOR EFFICIENCY FOR DIFFERENT SPEEDS [11].

4. TURBOCHARGER MODEL AND EFFICIENCY DEFINITIONS DESCRIPTION

The measurement of turbocharger maps in the gas stand can be done using different approaches. The main two approaches previously stated are hot and cold tests. In hot tests, the turbine inlet gas temperature is maintained high (similar to the exhaust gases temperature of the engine). Whereas, in cold tests here described, the temperatures of turbine inlet, oil inlet and compressor outlet are maintained at similar levels. Further, the turbocharger is externally insulated to minimize the external heat transfer. When a turbocharger is tested in hot conditions, the efficiency values of compressor and turbine are affected by heat transfer phenomena occurring during the tests. This is mainly due the high temperature differences between the different turbocharger elements. Fig 3 shows the idealized evolutions in enthalpy-entropy diagrams, where heat exchange processes are differently placed for compressor and turbine. Fig 3(a) shows that heat is added after the process of compressor compressing (adiabatically) the air and Fig 3 (b) shows that heat is subtracted in the turbine process before gas is expanded (adiabatically). It is worth highlighting that, as shown in Fig 3 (a), the entire heat transfer between the compressed air (T^{ad}_{TAir}) and metal node C are considered in the outlet of the compressor rotor [12]. These heat fluxes change the air temperature at the outlet of the compressor volute and the gas temperature at the inlet of the turbine stator. Therefore, the efficiencies calculated using volutes inlet and outlet temperatures would be different from pure adiabatic efficiency of the turbomachinery. In the cold tests, the measured efficiencies are less affected by heat transfer phenomena, so, the efficiencies obtained from this, also called, quasi-adiabatic test, will be closer to the adiabatic evolution.

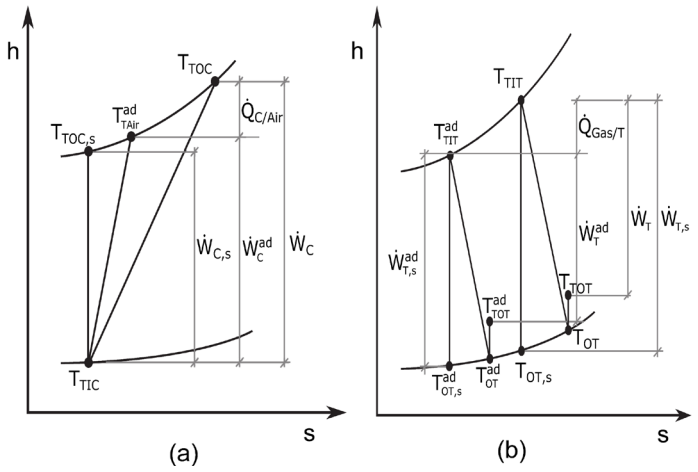

FIG 3: (A) COMPRESSOR: DIATHERMAL COMPRESSION PROCESS MODEL. (B) TURBINE DIATHERMAL EXPANSION PROCESS MODEL.

Several works have already published about heat transfer [12], [13], friction losses [14] and extrapolation models [15] of the turbocharger. These sub-models were implemented in one-dimensional reciprocating engine simulation software packages, to predict turbomachinery power outputs and outlet temperatures accurately. The holistic CMT turbocharger model was selected and integrated into the Kratzer Automation turbocharger gas stand control and acquisition system. The CMT turbocharger model [16] uses essentially geometrical data combined with physical and semi-empirical equations to decouple the heat transfer, and friction losses from efficiency maps and extrapolating the adiabatized maps to non-measured points.

The CMT turbocharger heat transfer model [16] is based on the electric analogy and, as shown in , has four working fluid nodes named as Gas, Air, Oil and W. The exhaust gas that enters the turbine is referred to as node Gas; this node is characterized by the turbine's measured inlet temperature shown in Fig 3 (b), (T_{TIT}). The adiabatically (but not isentropically) compressed air at the outlet diffuser of the compressor ($T_{\mathrm{TAir}}^{\mathrm{ad}}$), shown in Fig 3 (a), is the temperature shown in for node Air. Whereas nodes Oil and W are characterized by the lube oil (T_{OI}) and coolant liquid (T_{WI}) inlet temperatures. Further, there are five metal nodes: the turbine and compressor casings are simplified by one node each (T and C) and the remaining three nodes (H_1, H_2 and H_3) are considered for splitting the bearings housing as shown in scheme. The CMT model estimates the internal heat fluxes from fluid to metal nodes using the internal convection correlations described in [12]. For external convection (natural or forced) and radiation with ambient, the correlations described in [13] are used.

For conduction heat transfer from one metal node to the other metal node and to consider the thermal inertia at each node, the model described in [16] is used. Finally, friction losses in the lube oil are added as a power source to close the system's energy balance. The friction losses model computes the friction power in both radial and thrust bearings [14]. The different sub-models are run in real time while the turbocharger experimental points are being measured, generating adiabatized results by adding or subtracting heat fluxes [16], as sketched in the schemes of Fig 3 and . Also, the gas stand operator can ask for extrapolated maps from the measured points using the model described by [15].

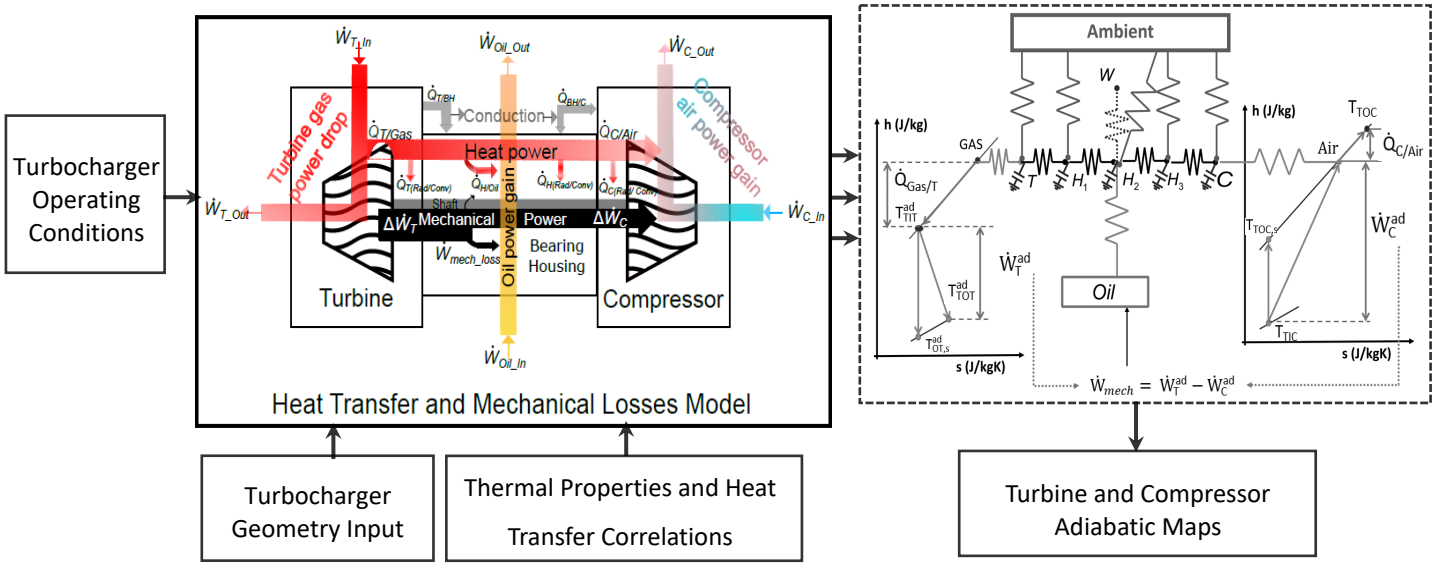

FIG 4: OVERVIEW OF THE HEAT TRANSFER CALCULATION METHODOLOGY IN A TURBOCHARGER TO OBTAIN THE ADIABATIC EFFICIENCY MAPS.

This way, the turbocharger gas stand automation and data acquisition system characterize thermally the turbocharger in-situ and during the experimental campaign and calculate adiabatized turbine and compressor efficiencies even at points not directly measured.

The SAE definition [10] of compressor efficiency is shown in Eqn. (2), i.e. the ratio of power between the isentropic compression process ($\dot{W}_{C,s}$) and actual process ($\dot{W}_C$). The actual process can only account for pure aerodynamic effects in the case of adiabatic tests ($\dot{W}_C^{ad}$). But, when a turbocharger is measured in a hot condition, the heat transfer effects in compressor influences the measured power as shows Eqn. (2) and Fig 3(a).

$$\eta_{C,\mathrm{hot}}^{\exp} = \frac{\dot{W}_{C,s}}{\dot{W}_C^{ad} + \dot{Q}_{C/Air}} \tag{2}$$

As the heat transfer model is applied in real time while measuring the hot maps, the internal heat flux between compressed air (T_{TAir}^{ad}) and metal node (C) are calculated using the convection correlation as described in [12].

Once, the compressor heat flux values are obtained by the model, that heat flux are discounted from the measured compressor power [16] then the system provides the adiabatized compressor efficiency as shown in Eqn. (3).

$$\eta_{C,ad}^{model} = \frac{\dot{W}_{C,s}}{\dot{W}_C^{ad}} \tag{3}$$

From turbocharger gas stand and using SAE standards [10], can also be directly calculated the values of different turbine efficiency definitions. The first efficiency definition is called net turbine efficiency or Effective Turbine Efficiency (ETE), and it is the efficiency used in SAE turbine maps provided by the turbocharger manufacturers. It compares total-to-total compressor power with the total-to-static isentropic power of the turbine, as shown in Eqn. (4).

$$\eta_{T,ETE}^{\exp} = \frac{\dot{W}_C}{\dot{W}_{T,s}} = \frac{\dot{W}_C^{ad} + \dot{Q}_{C/Air}}{\dot{W}_{T,s}} \tag{4}$$

Eqn. (4) shows that the ETE obtained from the hot tests are the mixture of different energy fluxes in a turbocharger [12]. It includes the effects of the heat transfer in compressor, turbine and the mechanical friction losses in the shaft. It is worth highlighting that the ETE definition (Eqn. (4)) uses "diathermal" turbine isentropic power ($\dot{W}_{T,s}$), because it includes heat flux ($\dot{Q}_{Gas/T}$), see Fig 3(b); instead of using "adiabatic" turbine isentropic power ($\dot{W}_{T,s}^{ad}$), that doesn't include heat flux ($\dot{Q}_{Gas/T}$), also see Fig 3(b). Since, at the turbine side, the entire heat transfer between the turbine gas inlet temperature (T_{TIT}) and metal node (T) are considered in the turbine volute (i.e., before gas expansion in the turbine stator). Therefore, $\dot{W}_{T,s}^{ad}$ is determined by the system (turbo model + gas stand) once the adiabatic total turbine inlet temperature (T_{TIT}^{ad}) is computed. This is done by subtracting the heat transfer that takes place on the turbine side ($\dot{Q}_{Gas/T}$), calculated using the heat transfer model (Fig 3). The rigorous definition of total-to-static turbine efficiency should compare only total-to-total adiabatic power of the turbine expansion with total-to-static isentropic expansion power, as shown in Eqn. (5), and can be directly called adiabatic turbine efficiency. This efficiency can be obtained from the turbocharger model after deducting the possible heat flux at the turbine side in the case of hot tests as explained before.

$$\eta_{T,ad}^{model} = \frac{\dot{W}_T^{ad}}{\dot{W}_{T,s}^{ad}} \tag{5}$$

Once the model discounts all the possible heat fluxes at the turbine and compressor side [16], the system provides the turbocharger mechanical efficiency as shown in Eqn. (6). If Eqn. (5) is multiplied by Eqn. (6), then the adiabatic ETE, without considering any heat transfer, is obtained, as shown in Eqn. (7).

$$\eta_{mech}^{model} = \frac{\dot{W}_C^{ad}}{\dot{W}_T^{ad}} \tag{6}$$

$$\eta_{T,ad}^{model} \cdot \eta_{mech}^{model} = \frac{\dot{W}_T^{ad}}{\dot{W}_{T,s}^{ad}} \cdot \frac{\dot{W}_C^{ad}}{\dot{W}_T^{ad}} = \frac{\dot{W}_C^{ad}}{\dot{W}_{T,s}^{ad}} \tag{7}$$

The differences between diathermal ETE from Eqn. (4) and adiabatic ETE from Eqn. (7) are better understood when comparing them at the light of the terms sketched at Fig 3(a) Further analysis of the turbocharger model and more equations relations can be read at [12] and [16].

5. ADVANTAGES FROM ON-LINE ADIABATIZATION OF TEST DATA OBTAINED FROM GAS STAND

In this work, two different turbochargers with VGT were selected to test them in the automation gas stand. First, hot external insulated tests were performed on the turbocharger named as T#1 under steady flow conditions. The primary objective of these tests is to decouple internal from external heat transfer by significantly minimizing the later, due to insulating the turbocharger unit externally. Therefore, the measured efficiencies are affected by only heat fluxes inside the turbocharger. Second turbocharger named as T#2 was tested under quasi-adiabatic conditions [2]. The internal heat fluxes between the turbocharger elements can be minimized by providing the lowest possible temperature gradient between the elements. External heat transfers are minimized by insulating the outside surface of the turbocharger. Therefore, quasi-adiabatic efficiencies can be calculated directly from measurements. Another objective is to decouple the heat transfer and the mechanical losses of the turbocharger when measuring oil temperatures. Therefore, energy absorbed by the lubrication oil will mainly come from heat generated by friction losses.

5.1. Hot Insulated Test Results

The hot external insulated tests were performed by setting operative conditions of the automation gas stand at a turbine inlet temperature of around 600 K. The bearing housing was cooled with water at 323 K, and oil inlet temperature was maintained at 363 K. T#1 turbocharger maps were obtained at 3 different VGT positions from 49 krpm to 170 krpm of compressor corrected speed and in between compressor choke and surge conditions, as shown in Fig 5(a). The different compressor corrected speeds were maintained constant in all the tested VGT positions.

Fig 5 (b) shows the turbine's reduced mass flow parameter for different VGT positions tested in the gas stand. As already discussed, the measured efficiency in both turbine and compressor will differ from adiabatic efficiency. It is due to the impossibility of decoupling from heat fluxes inside the turbocharger the fluids temperature drop due to expansion or compression [17].

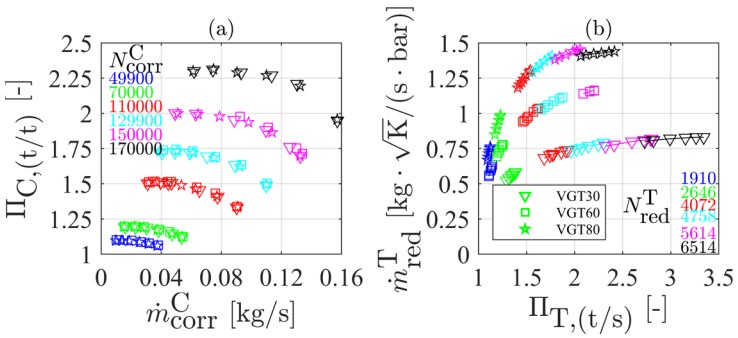

FIG 5: TURBOCHARGER T#1. (A) COMPRESSOR AND (B) TURBINE MAPS MEASURED IN HOT INSULATED CONDITIONS AT 3 DIFFERENT VGT (B) POSITIONS.

However, after the integration of the holistic turbocharger model with the gas stand automation and data acquisition system, the adiabatized efficiencies of turbine and compressor are obtained.

Fig 6 shows the turbocharger T#1 compressor efficiency results (Eqn. (2)) for three different VGT positions tested in the hot flow conditions versus the adiabatized efficiency (Eqn. (3)). Fig 6 shows how both compressor efficiencies are very similar from 110 krpm onwards, due to the small heat transfer in the compressor compared to compressor mechanical power. Further, the water cooling makes a thermal barrier from the turbine to the compressor. However, at the lowest compressor corrected speed (49 krpm), even with so active water cooling, the hot efficiency maps obtained from experiments do not represent by far the machine's aerodynamic (adiabatic) efficiency. It is due to the increment of relative heat transfer effects. At low speeds, the compressor is influenced mainly by the turbine inlet temperature and oil temperature in the bearing housing, increasing the compressor air outlet temperature. Consequently, the efficiency values obtained from hot tests decrease (Eqn. (2)). Thus, it can be concluded that the compressor efficiency obtained from hot test conditions provides only reliable results for high speeds.

Fig 7 shows the results of diathermal ETE (Eqn. (4)) obtained from the hot insulated tests and adiabatic ETE - as the product of adiabatic and mechanical efficiencies (Eqn. (7)) - calculated by the model. Fig 7 shows differences that are caused by twofold; the heat flux in the compressor ($\dot{Q}_{C/Air}$) and the different turbine isentropic power used in both definitions ($\dot{W}_{T,s}$ versus $\dot{W}^{ad}_{T,s}$), what is highly related with the heat flux in the turbine ($\dot{Q}_{Gas/T}$), see Fig 3(a), Eqn. (4) and Eqn. (7). Fig 7 shows that the difference between both ETEs is more important at lower compressor corrected speeds (i.e., lower turbine reduced speeds). At these speeds, the heat transfer to the compressor ($\dot{Q}_{C/Air}$) is very significant, as shown in Fig 6. In addition, it is erroneously computed as compressor power, therefore the adiabatic ETE is lower than the diathermal ETE. At high compressor corrected speeds, the differences are smaller, but the trend is clearly inverted. It is due to the heat transfer in the compressor side is negligible (see high turbocharger speeds at Fig 6) and what count here are the differences in the turbine isentropic power ($\dot{W}_{T,s}$ vs $\dot{W}^{ad}_{T,s}$). Attending to Eqn. (4) and Eqn. (7) definitions, the lower total-to-static isentropic power ($\dot{W}_{T,s}$ vs $\dot{W}^{ad}_{T,s}$) is, the higher the ETE. As can be deducted from Fig 3(b), the relative difference between both isentropic powers will be small at high expansion ratios. Therefore, only a slight difference in the efficiencies is shown at high corrected speeds and pressure ratios since $\dot{W}_{T,s}$ will be close to $\dot{W}^{ad}_{T,s}$.

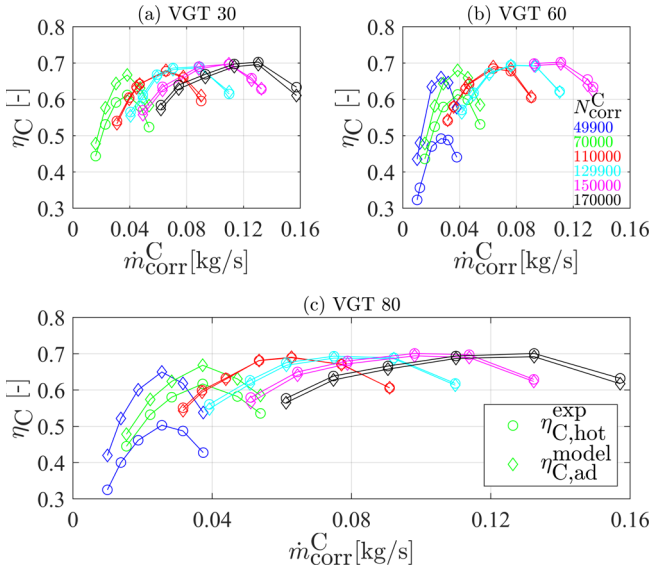

FIG 6: HOT INSULATED MEASUREMENTS OF COMPRESSOR EFFICIENCY V.S. THE ADIABATIZED COMPRESSOR EFFICIENCY FOR T#1

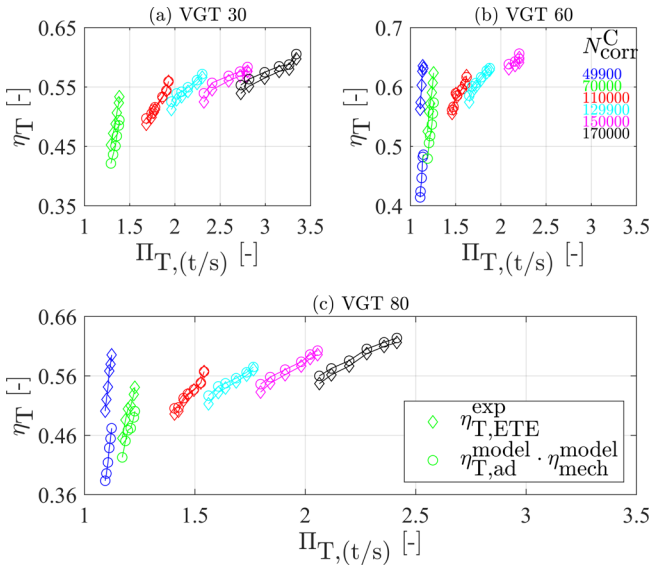

FIG 7: HOT INSULATED MEASUREMENTS OF DIATHERMAL E.T.E. V.S. ADIABATIC E.T.E. FOR T#1

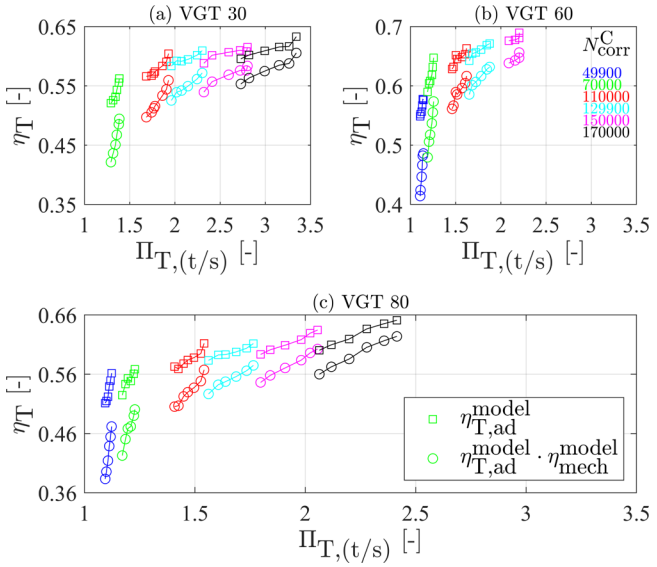

FIG 8: COMPARISON OF ADIABATIC TURBINE EFFICIENCY WITH ADIABATIC E.T.E. BOTH CALCULATED FOR T#1

Fig 8 shows the results of turbine adiabatic efficiency and adiabatic ETE obtained from the model. The comparison between these efficiencies (Eqn. (5) and Eqn. (7)) represents the impact of the turbocharger friction losses in the net turbine efficiency (adiabatic ETE). Fig 8 shows that the adiabatic efficiency is always higher in all the tested speeds and VGT positions than adiabatic ETE. The difference between both efficiencies is more noticeable at lower corrected speeds. The effect of mechanical friction losses in the turbocharger is more critical at low turbocharger speeds because the turbine and compressor power decrease faster than the mechanical power losses. These impacts in efficiency can be quantified on-line during turbocharger testing.

In addition, the upgraded turbocharger gas stand automation, with the turbocharger model, can quantify the heat fluxes balance between the turbocharger's parts. Therefore, it is possible to perform benchmarking analysis in this heat fluxes aspect when several turbochargers are measured in the gas stand at the same hot conditions. As an example, heat flux balances in T#1 are shown in Fig 9.

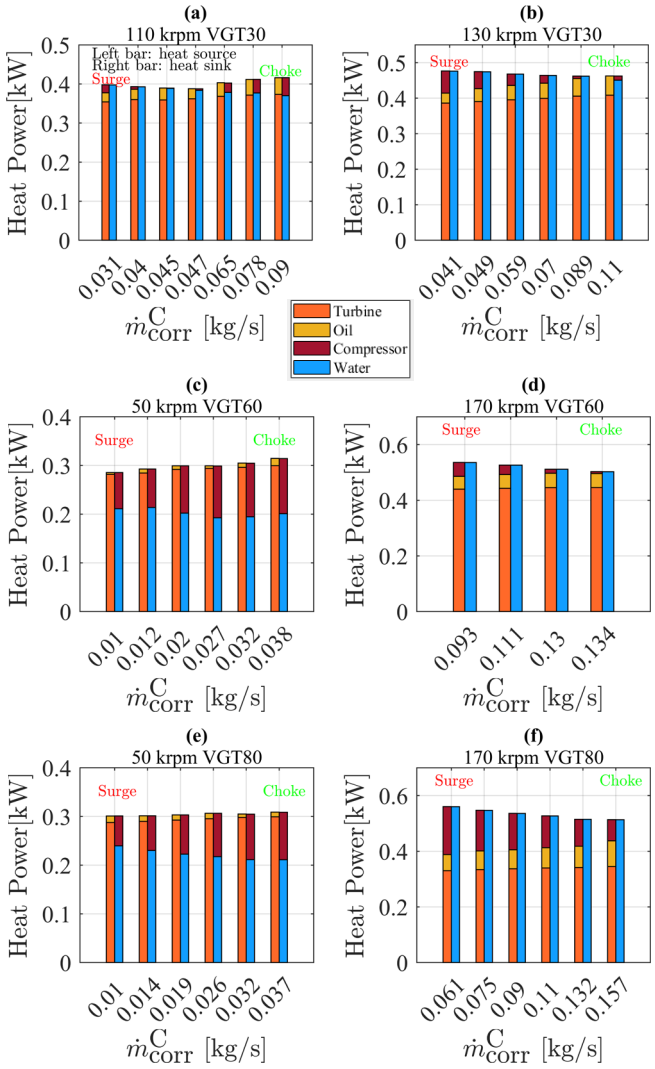

FIG 9: HEAT FLUXES BALANCE IN T#1 AT HOT INSULATED CONDITIONS

Fig 9 shows heat balances for lower and higher T#1 speeds and different VGT positions. The heat fluxes from (or towards) the four flows involved (turbine gas, compressor air, lubrication oil and cooling water) are interpreted by different bars in Fig 9. The left bar is the sum of all heats flowing from fluids to the turbocharger's metal parts (positive heat fluxes), and the right bar

is the sum of all heats flowing from metal parts to the turbocharger fluids (negative heat fluxes). As T#1 was tested at hot insulated conditions, the maximum temperature always corresponds to the turbine gas inlet. Therefore, the heat will always flow from the turbine gas inlet due to the second law of thermodynamics.

Fig 9 also shows that in turbocharger T#1 -water cooled- and at hot insulated conditions, the lubrication oil is always a heat source, and the cooling water is always a heat sink. The compressor air heat flux changes its direction depending on the operating conditions: at low speed, the compressor air absorbs heat from the turbine gas and the oil even with an active water-cooling system, see Fig 9 (c) and (e). But the compressor air becomes a heat source at high turbocharger speeds, and the water coolant works as the only heat sink, see Fig 9 (d) and (f). Further, it is also noticeable that there are intermediate speeds where we can see a transition. For example, in Fig 9 (a) and (b), the amount of heat compressor air receives or transmits mainly depends on the compressor working point (pressure ratio) for a given iso speed. When it is close to surge point, it is a heat source and the heat fluxes exchanged by the compressor air are positive (they are at right bars); but close to the choke limit heat fluxes are negative (they are at left bars) as in a heat sink.

In relative terms, the analysis of the different heat fluxes is shown in Fig 10 and Fig 11 for the VGT positions corresponding to 30% and 60% vane openings, respectively. Heat fluxes in compressor and turbine flows have been made dimensionless with respect to adiabatic powers, so does oil heat flux with respect to the calculated mechanical losses power. For both VGT positions the same general trend is observed. Heat fluxes through the turbine are relatively more important than they are in the compressor. Fig 10 (a) and Fig 11 (a) show peak values of around 42% for 70 krpm of corrected compressor speed whilst Fig 10 (b) and Fig 11 (b) peak values are around 10% for the same speed.

At the lowest corrected speed (49 krpm), Fig 11 (a) shows that peak values reached about 120%, it means more than half of the enthalpy drop measured at the turbine gas correspond to heat losses. Thus, at these low speed and low mass flow conditions the error of turbine adiabatic ETE could get to be really significant.

Heat fluxes in the oil are contained in a range between 25% at low speeds and 5% at intermediate speeds (Fig 10 (c) and Fig 11 (c)). It is clear a slight increasing trend with the compressor mass flow for every reduced speed. In the case of the higher speeds (over 110 krpm) the trend is quite independent of the speed, ranging from 5% for the lowest flows to 10% for the highest. A detailed explanation for this behavior is out of the scope of this work.

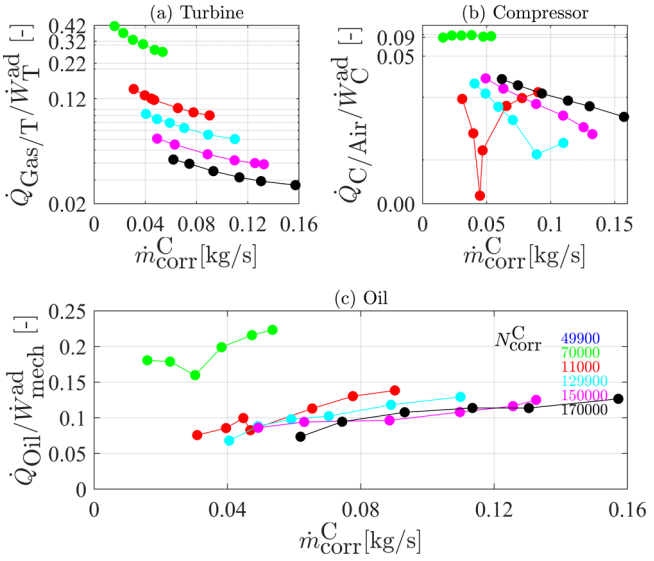

FIG 10: RELATIVE IMPORTANCE OF HEAT FLUXES IN T#1 AT 30% VGT POSITION & HOT INSULATED TESTS.

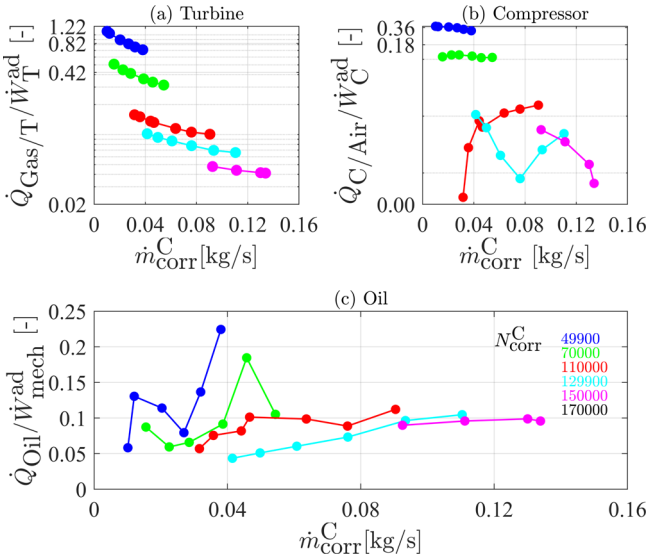

FIG 11: RELATIVE IMPORTANCE OF HEAT FLUXES IN T#1 AT 60% VGT POSITION & HOT INSULATED TESTS.

Fig 10 and Fig 11 show that the relative heat fluxes at turbine gas and oil flow have quite clear monotonous trends and, as already discussed they are always positive heat fluxes, see Fig 9. Nevertheless, Fig 9 bars show how the compressor air heat fluxes change from negative to positive as the turbocharger speed increases. Since negative values cannot be shown in logarithmic scales, Fig 10 (b) and Fig 11 (b) show sharp inflection points - close to 0% - for those speeds (110 & 130 krpm at Fig 10 (b)) where, inside them, the heat flux changes from negative (from compressor case metal to compressor air) to positive (from compressor air to case metal). These inflection points at 110 krpm and 130 krpm are also visible in Fig 9 (a) and Fig 9 (b) for

30% VGT position. Below those speeds, the compressor heat fluxes are always negative and over them are always positive.

5.2. Quasi-adiabatic Insulated Test Results

Quasi-adiabatic tests were done with T#2 under cold conditions with an externally insulated turbocharger. There were 168 points measured. The purposes of these tests in this work are twofold: on the one hand, checking model sensitivity to a change of fluid temperature conditions, and, on the other hand, quantifying small residual heat fluxes from adiabatic tests due to the model ability to detect and eventually correct them. The gas stand allowed to manage both turbine inlet and oil inlet temperatures, thus, they were set at each experimental point for being at the same value, and as similar as possible to the compressor outlet temperature, which varies according to the operating point [2]. A maximum temperature difference of 10 ºC was accepted, among any of these fluxes, during the experimental campaign. This was a trade-off between reducing heat fluxes between nodes and having long experimental times. Further, T#2 did not have an internal water cooling circuit, their quasi-adiabatic testing nature encouraged to avoid this circuit because of the heat to the water fluxes that would appear, as well as the fact that working with a not-so-high testing temperature as T#1 had would made the turbocharger to reduce the amount of cooling needed in order to not suffer severe damages.

To obtain a broad depiction of the T#2 map, 5 different VGT positions - from 20% to 80% - and 6 compressor corrected speeds, - from 45 krpm to 130 krpm - were measured. In all cases, measuring full range from choke to surge conditions in compressor map, as Fig 12 shows. Each one of the measured VGT positions maintained the same iso speed lines, allowing to measure the efficiency of the turbine for a wide range of vane openings. Since the working fluid was in cold conditions, it was decided not to increase the speed over 130 krpm to avoid big axial loading, because of the need of a high turbine inlet pressure to reach higher T#2 speeds. But, also, to avoid big oil deterioration, because of requirements of a high oil inlet temperature to keep the quasi-adiabatic conditions at high speeds.

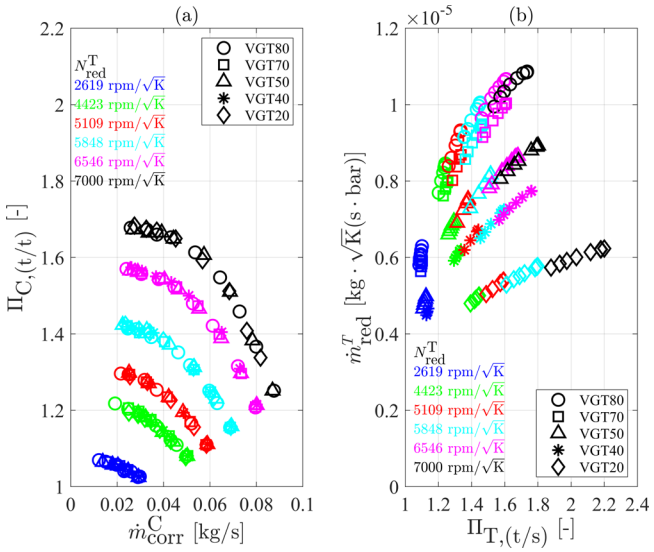

FIG 12: T#2 COMPRESSOR & 5 VGT MAPS MEASURED AT QUASI-ADIABATIC AND AT EXTERNALLY INSULATED CONDITIONS.

Fig 13 shows the experimental ETE (Eqn. (4)) versus the product of adiabatic and mechanical efficiencies (Eqn. (7)), acting as a representation of model effective turbine efficiency. By integrating the holistic model of the turbocharger within the control and data acquisition system of the gas stand, adiabatic and mechanical efficiencies have been obtained after discounting the proper heat fluxes as it has been shown in Eqns. (5)-(7). On the one hand, comparing different openings one can see how peak ETE is about 50% VGT opening. Also, that a higher expansion ratio is needed in the turbine to get the same compressor speed for the closer vane positions.

On the other hand, and as it could be expected, the differences between the experimental quasi-adiabatic ETE compared with the adiabatic ETE are almost negligible. By looking at low reduced speeds, a slightly higher difference is shown, and it is related to the relatively higher amounts of heat transferred to the compressor at these low speeds, as it was previously stated.

Fig 14 shows the differences between purely adiabatic turbine efficiency obtained from the model and the adiabatic ETE, with the same charts structure as in Fig 13. Fig 14 shows a clear trend no matter the vane opening that stands for an increase in mechanical efficiency at higher reduced speeds, since the pairs of points come closer. In this case, the analysis is like that of the hot testing for T#1. Mechanical efficiency is more affected by

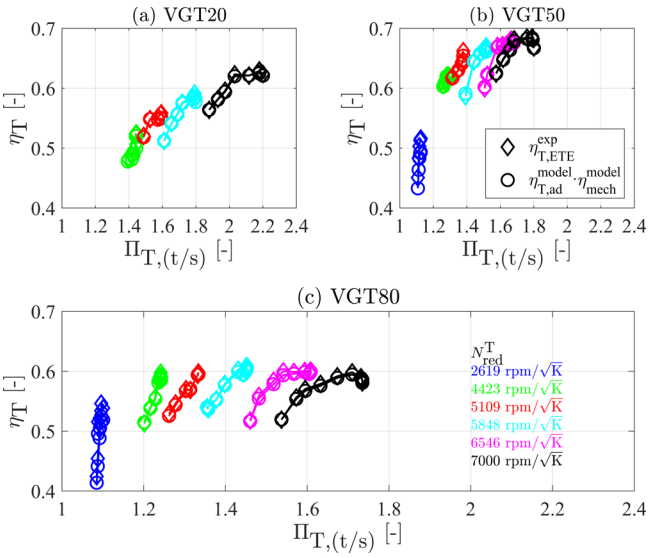

FIG 13: COMPARISON OF QUASI-ADIABATIC V.S. ADIABATIC E.T.E. FOR T#2.

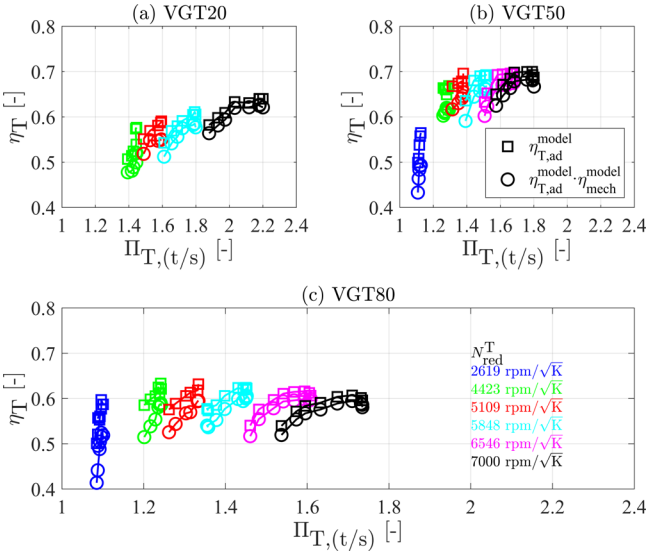

FIG 14: COMPARISON OF ADIABATIC TURBINE EFFICIENCY WITH ADIABATIC E.T.E. FOR T#2.

friction losses at low turbocharger speeds, meanwhile, for high reduced speeds, it becomes likely constant. Furthermore, heat transfer between the elements of the T#2 can be represented with the information provided by the model and the analysis must be done considering its quasi-adiabatic testing conditions. It means, that thermal insulation avoids heat fluxes to the ambient, meanwhile the lack of cooling water also prevents internal heat exchanges with this fluid. Hence, the balance would be raised between only three fluids: turbine gas, compressor air, and lubricating oil. Fig 15 shows the power balance for each experimental point along with the temperatures that led to the quasi-adiabatic conditions: turbine gas inlet, compressor air outlet and oil flow inlet temperatures. It can be checked how the limit of not overpassing 10 K difference was achieved.

Consequently, heat fluxes between elements were highly diminished since the whole system had similar temperatures. Fig 15 shows a few tens of W of heat flux exchanged, while Fig 9 shows some hundreds, i.e.: an order of magnitude less with the quasi-adiabatic tests. The analysis of Fig 15 shows that the value of matching temperatures to achieve quasi-adiabatic conditions is of utmost importance at higher speeds, that is why there is less uniformity along the same reduced iso-speed line. Anyway, the model can obtain the heat flow for each point, considering the influence of these temperatures, and correct its effect whatever the low value is.

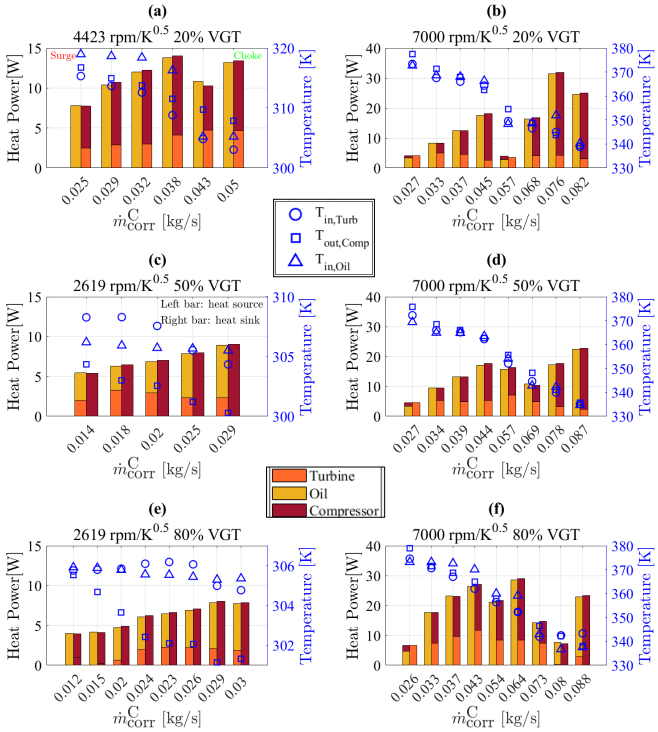

FIG 15: HEAT FLUX IN TURBOCHARGER WHEN TESTING IN GAS STAND AT QUASI-ADIABATIC INSULATED CONDITIONS.

Fig 15 shows high and low speeds for different VGT positions, and, for each tested point, it can be seen how the oil always acts as a heat source, releasing heat. Because the quasi-adiabatic test is based on matching oil inlet (coldest) temperature with the hottest from both turbine and compressor since oil temperature increases when passing through the bearings. Also, oil heat flux is increased as the compressor is close to surge at the lowest reduced speeds (Fig 15 (a) (c) (d)). Turbine gas and compressor air can act as sources or sinks depending on the speed and the testing conditions. At 50% and 80% VGT positions

and for the lowest reduced speed of 2619 rpm/K$^{0.5}$ (Fig 15 (c) (d)), the turbine releases heat, absorbed by the compressor, and this is due to punctual deviations in the quasi-adiabatic objective of matching the 3 temperatures.

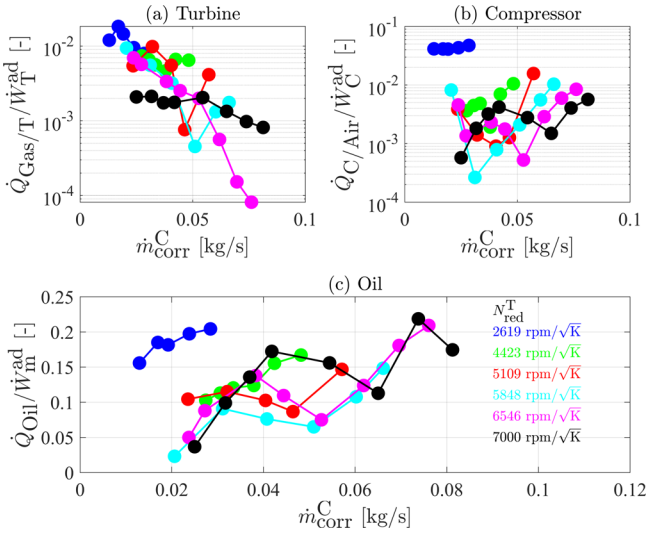

FIG 16: RELATIVE IMPORTANCE OF HEAT FLUX IN TURBOCHARGER AT VGT 50 POSITION FOR QUASI-ADIABATIC MEASUREMENTS.

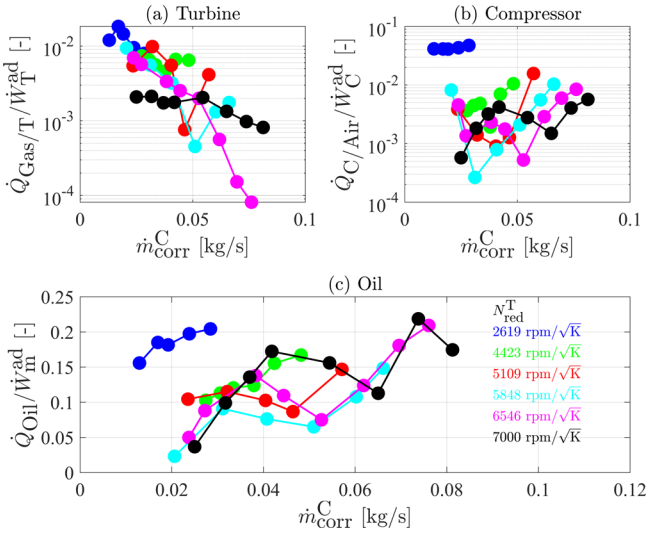

FIG 16 SHOWS HEAT FLUXES POWER AS A RATIO OF THE RESPECTIVE COMPONENT POWER. IN BOTH COMPRESSOR AND TURBINE HEAT FLUXES RATIOS ARE MOST OF THE TIME (EXCEPT FOR THE LOWEST SPEEDS) WELL BELOW 1 % OF THE RESPECTIVE COMPONENT POWER.

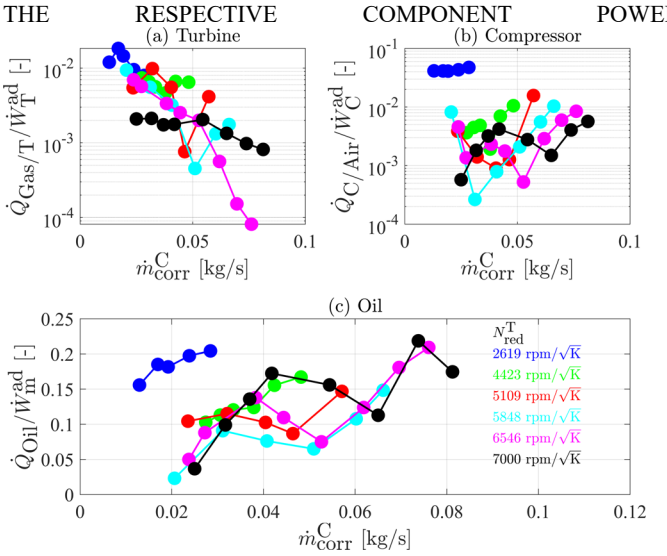

Fig 16 (b), and for 2619 rpm/K$^{0.5}$, shows how difficult it is achieving the adiabatic objective at very low speeds, with values close to 7 %.

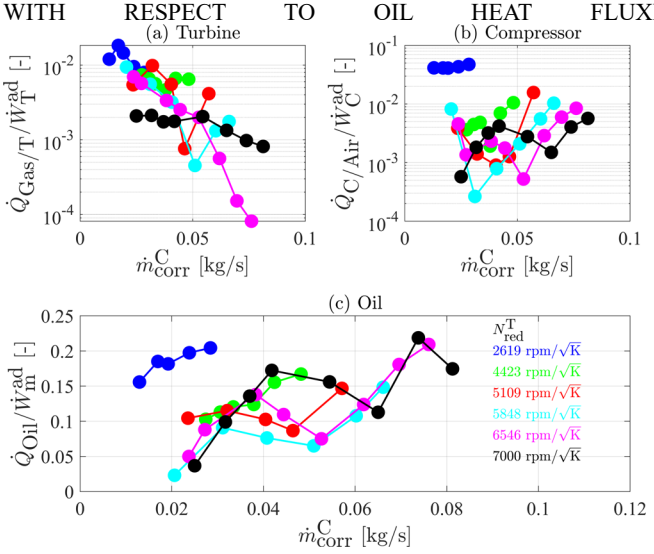

Fig 16 shows that they are again in a range between 5% and 25% of friction losses power, and with an increasing trend as the compressor corrected mass flow increases, as it was shown in T#1 tests.

6. REDUCING THE EXPERIMENT TIME BY MODEL EXTRAPOLATION

Once the actual adiabatic efficiency is calculated, the turbocharger gas stand automation system can also extrapolate the performance maps of the turbine in real time. The procedure that the system uses to extrapolate the performance maps of the turbine is described in [15]. The system extrapolates both, turbine reduced mass flow and adiabatic efficiency, in terms of

turbine reduced speed, expansion ratio, blade-to-jet speed ratio (BSR) and VGT position.

Fig 17 (a) shows the T#1 VGT reduced mass flow. The solid lines are the model extrapolation results, whereas the solid markers are the experimental points used by the model to produce the extrapolation. Fig 17 (b) shows the same maps, but the model uses only a fraction of the experimental points to get the extrapolated values. Hollow markers are the experimental points that are not used to fit the extrapolation model. Indeed, only one point per iso speed at the two edge VGT positions is used to fit all the maps. It means that, after measuring the whole turbine map for VGT 60%, the back-pressure valves downstream the T#1 compressor (see Fig 1) were held constantly. It was decided to fix T#1 back pressure load at central zone of its map, i.e.: the single point included per speed line at VGT 30% and 80% corresponds to the compressor map operating zone closer to its maximum efficiency, and with a wide margin from surge and choke conditions. Since then, back pressure valves are not changed any more during the rest of the test, measuring only one point per speed line for the VGT positions 30% & 80%.

The relative error of the model predictions when compared to the experimental points is shown below in the reduced mass flow charts of Fig 17 (a) and (b). The relative error of the reduced mass flow has been calculated as shown in Eqn. (8), and subtracting the points of equal expansion ratio.

$$\delta|_{\text{Turbine Map}} = \frac{\dot{m}^T_{\text{red}_{\text{model}}} - \dot{m}^T_{\text{red}_{\text{exp}}}}{\dot{m}^T_{\text{red}_{\text{exp}}}} \cdot 100 \qquad (8)$$

Fig 17 relative errors for extrapolated data points show very similar values for both techniques, with a maximum error of $\pm 2.5\%$ in the case of Fig 17 (a), measuring the whole data set, and a maximum relative error of -4% in the case of Fig 17 (b), measuring only 40 % of the original data set.

For the quasi-adiabatic insulated tests, Fig 18 (a) shows the turbine reduced mass flow for 3 different VGT positions, having chosen the biggest and the smallest openings as well as the mid-open position. Fig 18 (a) also shows the extrapolated reduced mass flow map with solid lines. In this case, the highest errors ($\pm 5\%$) appear for the lowest iso-speeds.

In Fig 18 (b) the number of experimental points used to fit the model is just one third of Fig 18 (a) data set, and VGT50 is responsible of 38 out of 58. It has been followed the same method for reducing the number of tested points previously described. Despite of this, the relative errors in Fig 18 (b) are quite the same as those in Fig 18 (a). What is more, Fig 18 (b) shows even lower relative errors than Fig 18 (a) for 50% VGT opening, probably due to the higher weight of these points over the total. The points from the other VGT openings were chosen also around the compressor peak efficiency area, which is a highly reliable measurement area from the compressor point of view.

Fig 19 (a to f) and Fig 20 (a to f) show the adiabatic efficiency points and the extrapolated efficiency maps for T#1 and T#2, respectively. And the relative error of adiabatic turbine efficiency, which has been calculated as shown in Eqn. (9), and in this case subtracting the points with the same experimental BSR.

$$\delta|_{\text{BSR}} = \frac{\eta^{\text{model}}_{\text{T,ad}} - \eta^{\text{exp}}_{\text{T,ad}}}{\eta^{\text{exp}}_{\text{T,ad}}} \cdot 100 \qquad (9)$$

Comparing between T#1, Fig 19 (a to f), and T#2, Fig 20 (a to f), efficiency data can be seen how peak efficiencies are reached at higher BSR in the case of T#2. This is the result of different turbine design objectives that influence efficiency behavior. It means T#2 has a VGT better matched for part load conditions of the turbocharged reciprocating internal combustion engine. Also, T#2 is smaller than T#1 according to the lower maximum reduced mass flow shown in Fig 18 vs Fig 17.

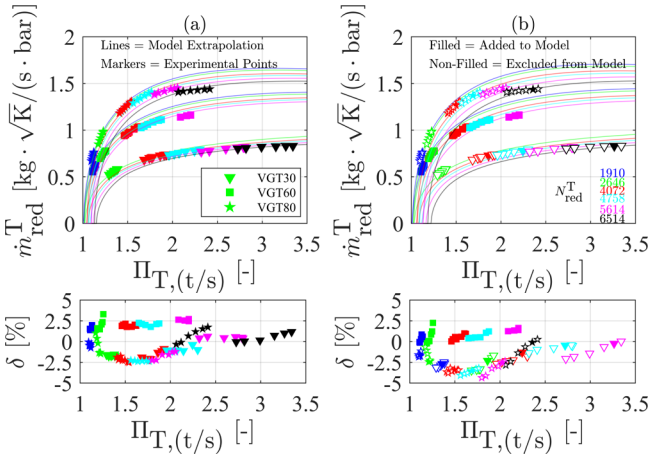

FIG 17: T#1 REDUCED MASS FLOW EXTRAPOLATION RESULTS FOR HOT INSULATED TESTS. (A) THE WHOLE DATA SET. (B) 40% OF THE DATA SET

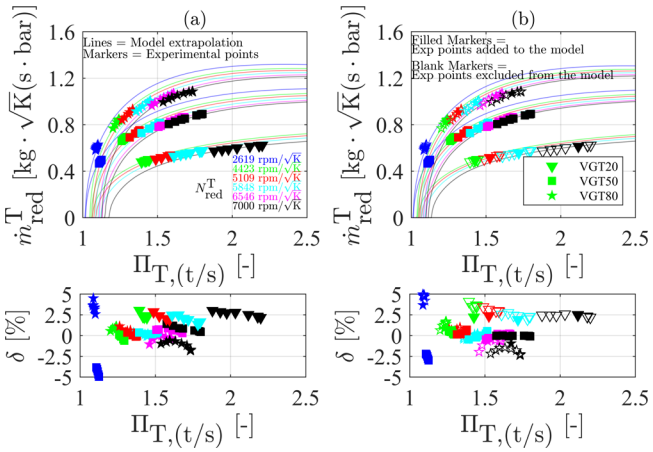

FIG 18: T#2 REDUCED MASS FLOW EXTRAPOLATION RESULTS FOR QUASI-ADIABATIC INSULATED TESTS. (A) THE WHOLE DATA SET. (B) 1/3 OF THE DATA SET.

With respect to the relative errors, most of the points are showing maximum relative errors in the range of ±5%. And both turbochargers are showing that the same trend in the relative errors of the extrapolation can be obtained when only a fraction of the original set of data points is measured. The method can be applied when measuring both hot and quasi-adiabatic maps and it is expected to provide a saving in turbine characterization time (and money) when measuring VGT maps. The technique would be to measure a complete turbine map for a mid-open VGT position, since compressor map must be measured at least once, (in our case 60% VGT for T#1 and 50% VGT for T#2), but just one point per iso-speed (wisely chosen as close to peak compressor efficiency area) at the remaining VGT positions.

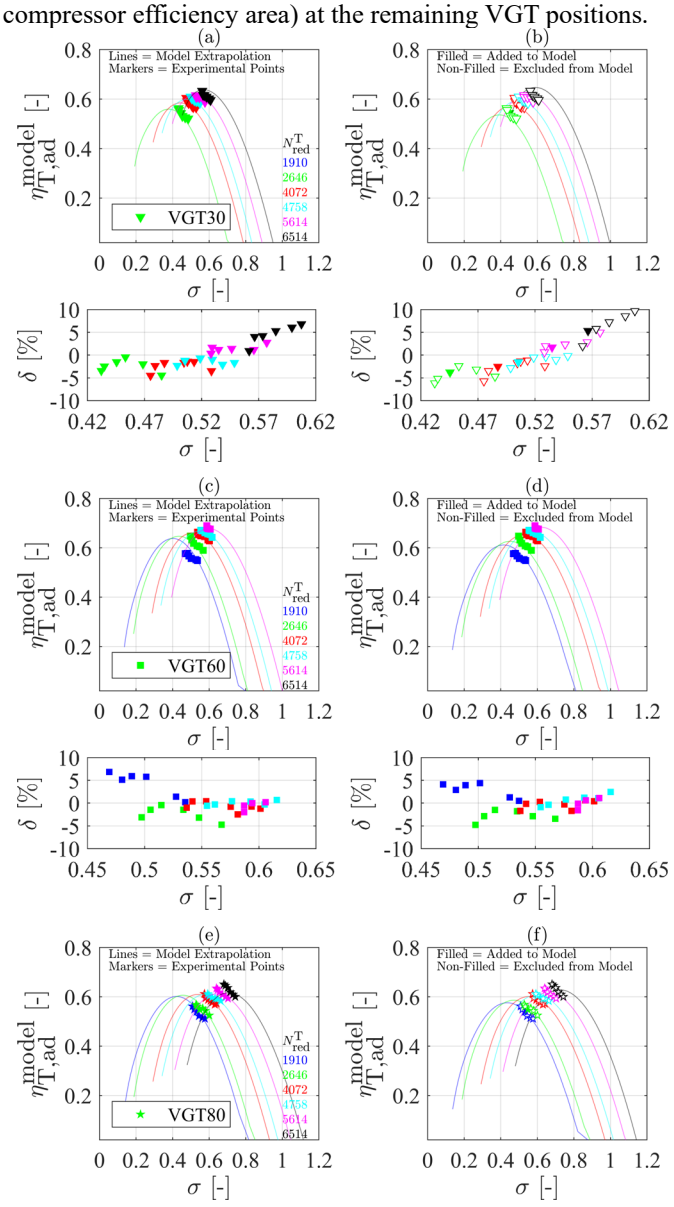

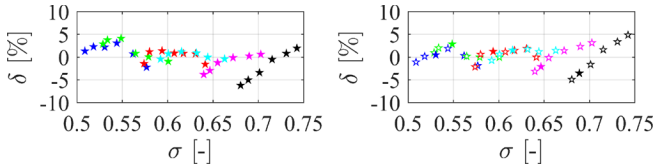

FIG 19: T#1 QUASI-ADIABATIC VGT EFFICIENCY EXTRAPOLATION RESULTS V.S. BLADE-TO-JET SPEED RATIO.

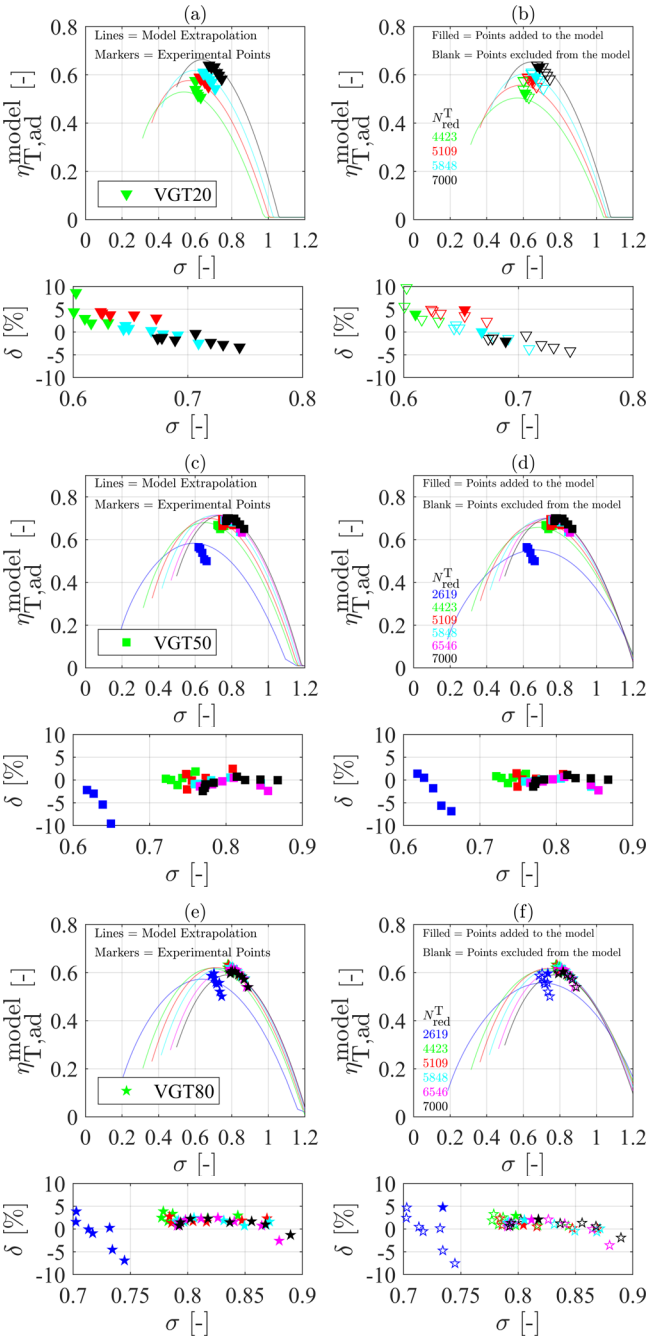

FIG 20: T#2 ADIABATIC VGT EFFICIENCY EXTRAPOLATION RESULTS V.S. BLADE-TO-JET SPEED RATIO.

7. MODEL-BASED DIAGNOSIS

During quasi-adiabatic tests, or when measuring extended maps using a closed loop in the compressor side, the turbocharger may endure damage over extended periods of time due to extreme axial loading or very high oil inlet temperature and, thus, very low dynamic viscosity. In these cases, metal to metal contact can be expected. This is not easily noticed just by looking at the usual turbocharger performance parameters such as the reduced or corrected speeds and mass flows or the efficiencies: if the amount of damage is small, the change in rotor dynamics may be not enough to affect to a big degree them. As the CMT turbocharger model computes hydrodynamic friction losses, it can be used as a digital twin model. It means, big discrepancies between the model output and the friction computed using the experimental data can be used as a sign of metal-to-metal contact in the bearings. Fig 21 shows the friction losses power computed by the model against the measured one in a quasi-adiabatic testing campaign with a pressurized closed-loop in the compressor side. In colors, the axial force is depicted, whereas the size of the markers is proportional to the oil inlet temperature.

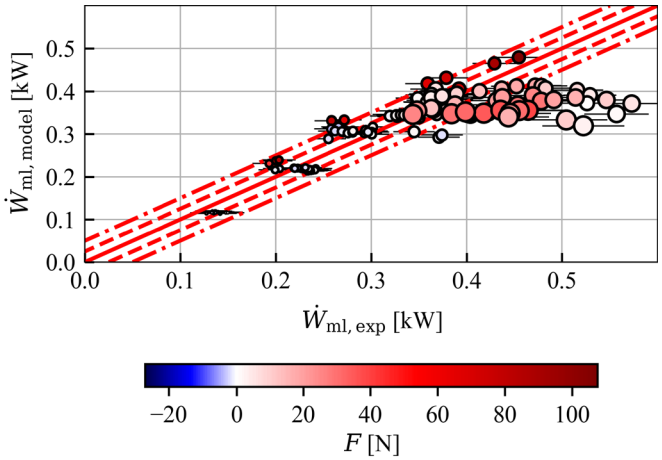

FIG 21: MECHANICAL LOSSES MEASURED AND COMPUTED BY THE MODEL IN QUASI-ADIABATIC TESTS (MARKERS SIZE IS PROPORTIONAL TO OIL INLET TEMPERATURE DURING QUASI-ADIABATIC TESTS)

The correlation of discrepancy (symptom of metal-to-metal contact) with axial load is not clear. Fig 21 shows that, on the one hand, there are mainly positive force (turbine pulling) and, on the other hand, there are white points (zero axial load) with big discrepancies and dark red points without discrepancy. However, always there are clear discrepancies at high powers (i.e. high speeds), which are the points where the oil inlet temperature was very high to ensure low amounts of internal heat fluxes. Oil samples were taken regularly during the experimental campaign, and they showed a huge increase of dynamic viscosity after measuring the points with huge discrepancies in mechanical losses prediction. Fig 22 shows such results, which are consistent with oil coke production due to the high temperatures as well as the presence of metal particles.

After making the experiments, the turbocharger unit was disassembled, showing scratches and damage in bearings. Fig 23 shows a detailed view of the thrust bearing: the rotating washer shows cracks produced after having metal-to-metal contact. This turbocharger unit had to be discarded due to the amount of damage sustained by the bearing system. By checking the difference between the measured friction power and the model friction power, an alarm can warn the gas stand operator of possible early damage when a given threshold is surpassed. This threshold must be set considering the uncertainty of the measurement in order not to produce too many false alarms. This method has the advantage that it can catch bearing metal-to-metal contact even when the axial force is relatively small but other effects are producing a loss of oil film, such as extreme temperatures or partial clogging of the oil feeding ducts.

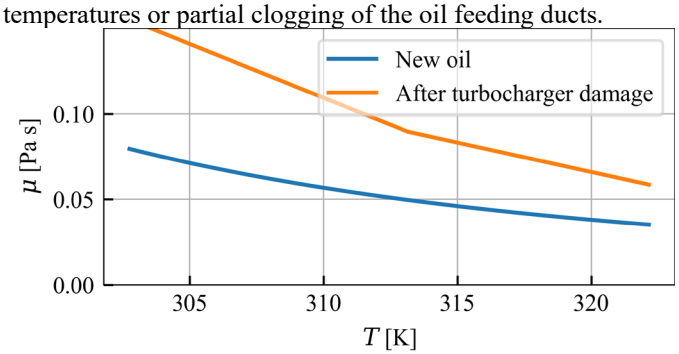

FIG 22 : OIL VISCOSITY ANALYSIS BEFORE (NEW OIL) AND AFTER QUASI-ADIABATIC TESTS (AFTER TURBOCHARGER DAMAGE)

FIG 23: DAMAGED THRUST BEARING AFTER QUASI-ADIABATIC TESTS

8. CONCLUSIONS

Integrating different heat transfer and mechanical losses models into the turbocharger gas stand control software and making them to run in real time while the points are being

measured, makes possible to obtain on-line the adiabatized efficiencies of turbine and compressor. Further, it can be used to easily benchmark the different turbocharger units by measuring them at operative conditions, different to their highest level of aerodynamic efficiencies, and provides the individual heat fluxes for analysis and comparison of said heat fluxes at the different elements of the turbochargers and between different brands.

By extrapolating the turbine map while measuring in the gas stand, the results can be compared on-line with that of the points that are being measured: the gas stand operator can decide to stop the experimental tests when the extrapolated results reach the objective level of accuracy. The rest of the map can then be filled by extrapolation, therefore, reducing the amount of time and resources needed to characterize the whole turbine map. It has the added benefit of reducing the amount of time expended in conditions very close to surge or very close to choke and the time used with the compressor operating in a pressurized, closed-loop circuit reducing the risk of damaging the turbocharger unit being characterized.

A final interesting aspect of using a digital twin while measuring in a gas stand are the extra diagnosis capabilities. In this work, it has been used, to show as an example, to diagnose bearing damage during a quasi-adiabatic testing campaign with a compressor pressurized closed-loop and low viscosity oil. It has been shown the ability for detecting oil film loss due to different phenomena and discriminating among them, like the oil coking at high temperatures versus the axial load.

REFERENCES

[1] A. Romagnoli *et al.*, “A review of heat transfer in turbochargers,” *Renewable and Sustainable Energy Reviews*, vol. 79. Elsevier Ltd, pp. 1442–1460, Nov. 01, 2017, doi: 10.1016/j.rser.2017.04.119.

[2] J. R. Serrano, F. J. Arnau, L. M. García-Cuevas, A. Gómez-Vilanova, S. Guilain, and S. Batard, “A Methodology for Measuring Turbocharger Adiabatic Maps in a Gas-Stand and Its Usage for Calibrating Control Oriented and One-Dimensional Models at Early ICE Design Stages,” *J. Energy Resour. Technol.*, vol. 143, no. 4, Apr. 2021, doi: 10.1115/1.4048229.

[3] U. Tomm, S. Weiske, A. Coksen, Y. Rafaa, and S. Münz, “Validation of a Heat Transfer Prediction Approach Inside Turbochargers and its Application on Turbocharged Engine Performance Analysis,” *Vol. 8 Microturbines, Turbochargers Small Turbomachines; Steam Turbines*, p. V008T26A003, 2017, doi: 10.1115/GT2017-63195.

[4] S. Zhu, K. Deng, and S. Liu, “Modeling and extrapolating mass flow characteristics of a radial turbocharger turbine,” *Energy*, vol. 87, pp. 628–637, Jul. 2015, doi: 10.1016/j.energy.2015.05.032.

[5] X. Llamas and L. Eriksson, “Control-Oriented Compressor Model with Adiabatic Efficiency Extrapolation,” *SAE Int. J. Engines*, vol. 10, no. 4, 2017, doi: 10.4271/2017-01-1032.

[6] M. Deligant, P. Podevin, and G. Descombes, “Experimental identification of turbocharger mechanical friction losses,” *Energy*, vol. 39, no. 1, pp. 388–394, 2012, doi: 10.1016/j.energy.2011.12.049.

[7] R. D. Burke, C. D. Copeland, T. Duda, and M. A. Rayes-Belmote, “Lumped capacitance and three-dimensional computational fluid dynamics conjugate heat transfer modeling of an automotive turbocharger,” *J. Eng. Gas Turbines Power*, vol. 138, no. 9, Sep. 2016, doi: 10.1115/1.4032663.

[8] M. Lang, T. Koch, T. Eggert, R. Schifferdecker, and J. P. Watson, “A holistic consideration of turbocharger heat transfer analysis and advanced turbocharging modeling methodology in a 1D engine process simulation context,” *Automot. Engine Technol.*, vol. 5, no. 3–4, pp. 113–136, Dec. 2020, doi: 10.1007/s41104-020-00062-1.

[9] J. R. Serrano, P. Olmeda, A. Tiseira, L. M. García-Cuevas, and A. Lefebvre, “Theoretical and experimental study of mechanical losses in automotive turbochargers,” *Energy*, vol. 55, no. 0, pp. 888–898, 2013, doi: 10.1016/j.energy.2013.04.042.

[10] Society of Automotive Engineers. SAE-Standard J1826, “Turbocharger Gas Stand Test Code.” SAE, Warrendale, 1995.

[11] H. Mai, “Herausforderungen und Ansätze zur Optimierung der Turboladerkennfeldvermessung auf Heißgasprüfständen,” *Salomon, A., Jander, B., Savic, B. (Hrsg.): Spannungsfeld Fahrzeugantriebe - Gedenkschrift für Prof. Dr.-Ing. Roland Baar*. Berlin: Universitätsverlag der TU Berlin, pp. 518–535, 2020, doi: 10.14279/depositonce-9822.

[12] J. R. Serrano, P. Olmeda, F. J. Arnau, M. A. Reyes-Belmonte, and H. Tartoussi, “A study on the internal convection in small turbochargers. Proposal of heat transfer convective coefficients,” *Appl. Therm. Eng.*, vol. 89, pp. 587–599, 2015, doi: 10.1016/j.applthermaleng.2015.06.053.

[13] F. Payri, P. Olmeda, F. J. Arnau, A. Dombrovsky, and L. Smith, “External heat losses in small turbochargers: Model and experiments,” *Energy*, vol. 71, pp. 534–546, 2014, doi: 10.1016/j.energy.2014.04.096.

[14] J. R. Serrano, P. Olmeda, A. Tiseira, L. M. García-Cuevas, and A. Lefebvre, “Importance of Mechanical Losses Modeling in the Performance Prediction of Radial Turbochargers under Pulsating Flow Conditions,” *SAE Pap. 2013-01-0577*, pp. 729–738, 2013, doi: 10.4271/2013-01-0577.

[15] J. R. Serrano, F. J. Arnau, L. M. García-Cuevas, A. Dombrovsky, and H. Tartoussi, “Development and validation of a radial turbine efficiency and mass flow model at design and off-design conditions,” *Energy Convers. Manag.*, vol. 128, pp. 281–293, 2016, doi: 10.1016/j.enconman.2016.09.032.

[16] J. R. Serrano, P. Olmeda, F. J. Arnau, and V. Samala, “A holistic methodology to correct heat transfer and bearing friction losses from hot turbocharger maps in order to obtain adiabatic efficiency of the turbomachinery,” *Int. J. Engine Res.*, 2019, doi: 10.1177/1468087419834194.

[17] B. Sirakov and M. Casey, “Evaluation of Heat Transfer Effects on Turbocharger Performance,” *J. Turbomach.*, vol. 135, no. 2, p. 021011, 2012, doi: 10.1115/1.4006608.